Supplementary Material for

The Influence of the Framework Core Residues on the Biophysical Properties of Immunoglobulin Heavy Chain Variable Domains

Annemarie Honegger, Alain Daniel Malebranche, Daniela Röthlisberger,
and Andreas Plückthun*

Biochemisches Institut der Universität Zürich
Winterthurerstrasse 190
CH-8057 Zürich
Switzerland

*corresponding author.
Email address: plueckthun@bioc.uzh.ch

Present addresses:
A.D.M., The University of British Columbia School of Medicine, Class of 2011, Vancouver, BC V6T 1Z3, Canada;
D. R., University of Washington, Department of Biochemistry, HSB J555, Box 357350, Seattle, WA 98195, USA

Keywords: antibody engineering; immunoglobulin variable domains; framework 1 structure; scFv fragment; stability

Additional information about denaturant-induced denaturation of the scFv fragments studied

Tryptophan fluorescence as spectral probe for the unfolding of the scFv. The scFv fragments huV$_\kappa$3-huV$_H$3, huV$_\kappa$3-huV$_H$3•MocB and huV$_\kappa$3-huV$_H$3•1 contain 5 Trp residues, a sixth fully buried Trp is present in the lower core of the V$_H$ domain of huV$_\kappa$3-huV$_H$3•1 (Figure S1). Comparison of the spectra of the native and denatured isolated huVκ3 and huV$_H$3 domains and of the scFv composed of these domains suggests that the conserved core Trp L43 and Trp H43 are highly quenched in the native domains (Jäger *et al.*, 2001). Thus, the fluorescence intensity increases when the isolated huVκ3 and huV$_H$3 domains unfold. However, the specific fluorescence of the scFv is higher than the sum of the fluorescence of the two isolated domains. This is due to the contribution of the three V$_H$ tryptophan residues buried in the interface between the between the V$_L$ and the V$_H$ domain, Trp H54 (conserved), H109 (CDR-H3) and H139 (conserved). Their contribution is higher when they are buried in the domain interface (native scFv) than when these residues are solvent exposed (isolated domains). Upon domain dissociation, not only does the fluorescence quantum yield of these interface Trp residues decrease, but also the fluorescence maximum shifts from lower wavelengths to about 350 nm, the typical value for exposed tryptophan residues (Schmid, 2005).

Figure S2 compares the spectra of native and refolded huV$_\kappa$3-huV$_H$3 to those of the three core-grafted constructs. Spectra were recorded at 0 - 0.2 M GdmCl and at 4.9 - 5.1 M GdmCl. The emission maxima λ_{max} of the native and denatured state are listed in Table ST3. The decreased fluorescence quantum yield of the three interface Trp more or less balances the increased quantum yield of the conserved core Trp. As a result, the total fluorescence yield shows no drastic change upon denaturation, although the peak fluorescence intensity of the native state could not be determined with great precision. In Figure S3, the spectra of the denatured scFv are normalized to the maximal fluorescence intensity (Figure S3) and superimposed. This immediately demonstrates that not only the wavelength of the emission maximum, but also the shapes of the spectra of the denatured scFv are very similar. This finding is not compatible with the large differences in the amount of residual structure in huV$_\kappa$3-huV$_H$3 compared to the other constructs. However, such large differences would have

to be postulated if the denaturation curves were to be interpreted according to a two-state model (see main text).

Equilibrium unfolding curves. True two-state unfolding behavior of an scFv is the exception rather than the rule, particularly for scFv that require high denaturant concentrations to unfold, and it is predominantly seen in scFv that are composed of domains that have low intrinsic stability but are stabilized to a significant extent in the scFv (see below, Figure S6). We are, therefore, skeptical about the $\Delta G_{(H2O)}$-values derived from such extrapolations in view of the the very different m-values obtained for very similar constructs.

We thus prefer a qualitative interpretation of the unfolding curves: the unfolding curves of three of the four constructs, huV$_\kappa$3-huV$_H$3•MocB, huV$_\kappa$3-huV$_H$3•1 and huV$_\kappa$3-huV$_H$3•5, are roughly parallel in the range of their respective unfolding transitions, with m-values approaching the values expected for a two-state unfolding. The qualitative ranking of the three curves remains the same throughout the transition range. If the three spectra are compared at the same denaturant concentration, the spectral characteristics of huV$_\kappa$3-huV$_H$3•1 and huV$_\kappa$3-huV$_H$3•5 are closer to the denatured state than those of huV$_\kappa$3-huV$_H$3•MocB. The unfolding curve of the forth scFv, huV$_\kappa$3-huV$_H$3, clearly shows a different slope than the other three curves — it starts unfolding at roughly the same denaturant concentration as huV$_\kappa$3-huV$_H$3•5, but reaches the fully unfolded state at a significantly higher denaturant concentration than the other three constructs. As we will argue below, this indicates a hidden intermediate.

For our constructs, this qualitative picture does not depend on the way the spectral shift has been determined (Figure S4). We compared three different methods: (i) center of spectral mass, which does not imply a specific shape of the spectrum, but is sensitive to differences in the quantum yield between the native and the unfolded state, (ii) a gaussian fit which assumes symmetry of the fluorescence peak, which may not be the case for the native state of scFv that may contain both fully buried and highly solvent accessible tryptophan residues, (iii) and fit of the spectra by a Taylor series (Monsellier and Bedouelle, 2005).

For the three chimeric constructs the ranking by $\Delta G_{(H2O)}$-values, determined from these curves (Tables ST1 and ST2), confirm the qualitative ranking with 11.2 kcal/mol (m = 5.1

kcal·L/mol^2) for huV$_\kappa$3-huV$_H$3•1, 13.0 kcal/mol (m = 5.5 kcal·L/mol^2) for huV$_\kappa$3-huV$_H$3•5 and 17.2 kcal/mol (m = 6.6 kcal·L/mol^2) for huV$_\kappa$3-huV$_H$3•MocB. While the different methods of determining the spectral fit lead to slight differences in the exact values of the thermodynamic parameters, these difference are within the experimental error and do not affect the ranking of the construct. However, a two state fit of the unfolding curve of huV$_\kappa$3-huV$_H$3 results in an extrapolation to a $\Delta G_{(H2O)}$ of only 6.6 kcal/mol (m = 2.5 kcal·L/mol^2) due to the very low m-value, which is not consistent with the superior functional and thermal stability observed for this scFv.

Corrective terms involving the curvature of the spectra at their respective λ_{max} introduced by (Monsellier and Bedouelle, 2005) to compensate for the deviation from linearity of the relation between λ_{max} and the fraction of unfolded molecules only account for 0.1 - 0.3 kcal/mol and have no effect on the ranking (Table ST3). These corrective turns are supposed to correct both for the different peak width of the spectrum and the different fluorescence quantum yield of the native and the denatured state. As the comparison of the normalized spectra shows (Figure S3), the difference between the shape of the spectra of the native and of the denatured state is very similar for all four constructs. In contrast, the differences in quantum yield are obscured by the variations in absolute intensity (due, e.g., to light scattering effects or concentration errors). This can be seen by the fact that the relative peak intensities differ in spectra taken from the unfolding and the refolding curve of the same construct under the same conditions (Figure S2), while the peak shape remains the same (Figure S3).

The midpoint of the equilibrium unfolding curve of the scFv fragment huV$_\kappa$3-huV$_H$3 ([GdmCl]$_{50}$ = 2.6 M) is equal or lower than that of the isolated huV$_H$3 domain ([GdmCl]$_{50}$ 2.7 M (Ewert *et al.*, 2003) and this study), which is typical of an scFv in which the unfolding of the two domains is not stringently coupled. The isolated huV$_\kappa$3 domain unfolds with a [GdmCl]$_{50}$ of 2.3 M ((Ewert *et al.*, 2003) and this study). Due to aggregation of the material at low denaturant concentrations, interpretation of the unfolding curve of huV$_H$3•MocB can only be qualitative, as the fit of a pre-transition baseline was very unreliable. Comparison of the data points at higher denaturant concentrations to the unfolding curve of huV$_H$3 was found to be consistent with a curve that is parallel to the unfolding curve of huV$_H$3, but shifted to 0.4 M lower GdmCl concentration. This leads to an estimate of [GdmCl]$_{50}$ of approximately 2.3 M for the isolated V$_H$ domain. If this is correct, the midpoint for the unfolding of 2.7 M for

the scFv indicates an scFv in which both domains benefit from the association, indicating cooperative unfolding. Isolated domains huV$_H$3•1 and huV$_H$3•5 could not be produced in sufficient amounts and monomeric state to characterize of their unfolding curves.

Based on previous studies (Wörn and Plückthun, 1999; Wörn *et al.*, 2000; Jäger *et al.*, 2001; Röthlisberger *et al.*, 2005), we suggest that true two-state unfolding behavior of an scFv is the exception rather than the rule, and is predominantly seen in scFv composed of domains that have low intrinsic stability but are stabilized to a significant extent in the scFv (Figure S6a). For scFv with fairly high stabilities, unfolding curves like those depicted in Supplementary Figure S6b and S6d are more frequent: curves that show no discernable intermediate, but are characterized by a low m-value and a [GdmCl]$_{50}$ intermediate between those of the isolated V$_L$ and V$_H$ domain. If the difference between the intrinsic stabilities of the isolated V$_L$ and V$_H$ domain is sufficiently large, an stable intermediate in which the less stable domain is unfolded and the more stable one remains folded may present itself at intermediate denaturant concentrations (Figure S6c).

The equilibrium unfolding curve of scFv fragment huV$_\kappa$3-huV$_H$3 is clearly not compatible with two-state equilibrium unfolding, while for the other three constructs the case is not that clear, as their m-values are closer to the expected value. This is not likely to be due to a selective destabilization of the V$_L$/V$_H$ interface in the huV$_\kappa$3-huV$_H$3 construct, compared to the other three constructs: all residues whose side-chains contribute to this interface are identical in all four constructs. Furthermore, the main-chain hydrogen bonding between the strands of the β-sheet does not allow local changes of the backbone conformation.

In scFv that show a clear unfolding intermediate (Figure S6c), this intermediate represents a state where the variable domain with lower intrinsic stability is unfolded, while the domain with higher intrinsic stability remains folded and unfolds at the same denaturant concentration as the isolated domain (see Jäger *et al.*, 2001 for an example where the stability of V$_H$ was limiting, Wörn and Plückthun, 1999; Wörn *et al.*, 2000 and Röthlisberger *et al.*, 2005 for a series of constructs in which V$_L$ has been shown to be the first domain to unfold). The unfolding transition of the weaker domain is shifted to higher denaturant concentration compared to the isolated domain by the stabilizing influence of the V$_L$/V$_H$ interface. Such a clear step in the unfolding trace is only seen if denaturant concentrations where the first

unfolding transition is essentially complete and the second transition has not yet started is well separated. In cases where this range is narrower and the unfolding transition of the interface-stabilized weaker domain overlaps that of the stronger domain (Figure 6b), the combined unfolding trace resembles a two-state transition with decreased m-value and a midpoint intermediate between those of the two component domains. The smaller the gap between two individual transitions, the steeper this combined unfolding trace becomes. As a result, we find that starting from an scFv like the one depicted in Figure 6b, introduction of stabilizing mutations into the weaker domain will increase the apparent $[D]_{50}$, $\Delta G_{(H2O)}$ and m-value derived from a two-state fit. Introduction of *stabilizing* mutation into the stronger domain will increase the apparent $[D]_{50}$, but at the same time decrease the apparent m-value, which can lead to a *decrease* of the apparent $\Delta G_{(H2O)}$. Introduction of *destabilizing* mutations into the more stable domain will decrease the apparent $[D]_{50}$, but increases the m-value derived from a two-state fit, and therefore, paradoxically, *increases* the apparent $\Delta G_{(H2O)}$. The more stable an scFv is, the farther the extrapolation from $\Delta G_{(D50)}$ to $\Delta G_{(H2O)}$ has to reach beyond the relevant data points that contribute to the fit of the m-value, increasing the likelihood that even small changes of the m-value cancel the influence of the shift of $[D]_{50}$ on $\Delta G_{(H2O)}$.

The increased cooperativity of the scFv containing the chimeric V_H domains compared to huV$_\kappa$3-huV$_H$3 suggests a decreased difference between the intrinsic stabilities of V_L and V_H in these constructs as a consequence of a reduction of the intrinsic stability of these V_H domains. The decreased $[D]_{50}$ values for huVκ3-huV$_H$3•1 and huVκ3-huV$_H$3•5 compared to huVκ3-huV$_H$3•MocB and huVκ3-huV$_H$3 point in the same direction. An alternative explanation, blaming the low cooperativity observed for huV$_\kappa$3-huV$_H$3 on a destabilization of the V_L/V_H interface in this particular construct is highly unlikely, since the V_L domain and the V_H residues contributing to the V_L/V_H interface are identical in all four constructs, and the main-chain hydrogen bonding between the strands of the V_H β-sheet that supports the interface residues does not allow major changes of the backbone conformation.

We conclude that the increased cooperativity of huVκ3-huV$_H$3•MocB is a sign of a decreased intrinsic stability of huV$_H$3•MocB compared to huV$_H$3. Therefore, in the context of the huV$_H$3 CDRs, the huV$_H$3 consensus framework is more stable than the huV$_H$3•MocB chimera, while in the context of the Moc31-derived CDRs, the huV$_H$3•MocB chimeric framework was more

stable than the consensus framework. This difference in the stability ranking between the two frameworks can be explained by a different amount of steric strain between framework and CDRs.

References

Creighton, T.E. (1997). Protein Structure: A Practical Approach, 2nd. Edition ed. Oxford University Press.

Ewert, S., Huber, T., Honegger, A. and Plückthun, A. (2003) *J. Mol. Biol.,* **325**, 531-553.

Jäger, M., Gehrig, P. and Plückthun, A. (2001) *J. Mol. Biol.,* **305**, 1111-1129.

Monsellier, E. and Bedouelle, H. (2005) *Prot. Eng. Des. & Sel.,* **18**, 445-456.

Röthlisberger, D., Honegger, A. and Plückthun, A. (2005) *J. Mol. Biol.,* **347**, 773-789.

Schmid, F. (2005). Spectroscopic techniques to study protein folding and stability., Vol. 1, Protein Folding Handbook, edited by J. Buchner and T. Kiefhaber, pp. 22-44. KGaA: WILEY-VCH Verlag GmbH & Co. .

Wörn, A., Auf der Maur, A., Escher, D., Honegger, A., Barberis, A. and Plückthun, A. (2000) *J. Biol. Chem.,* **275**, 2795-2803.

Wörn, A. and Plückthun, A. (1999) *Biochemistry,* **38**, 8739-8750.

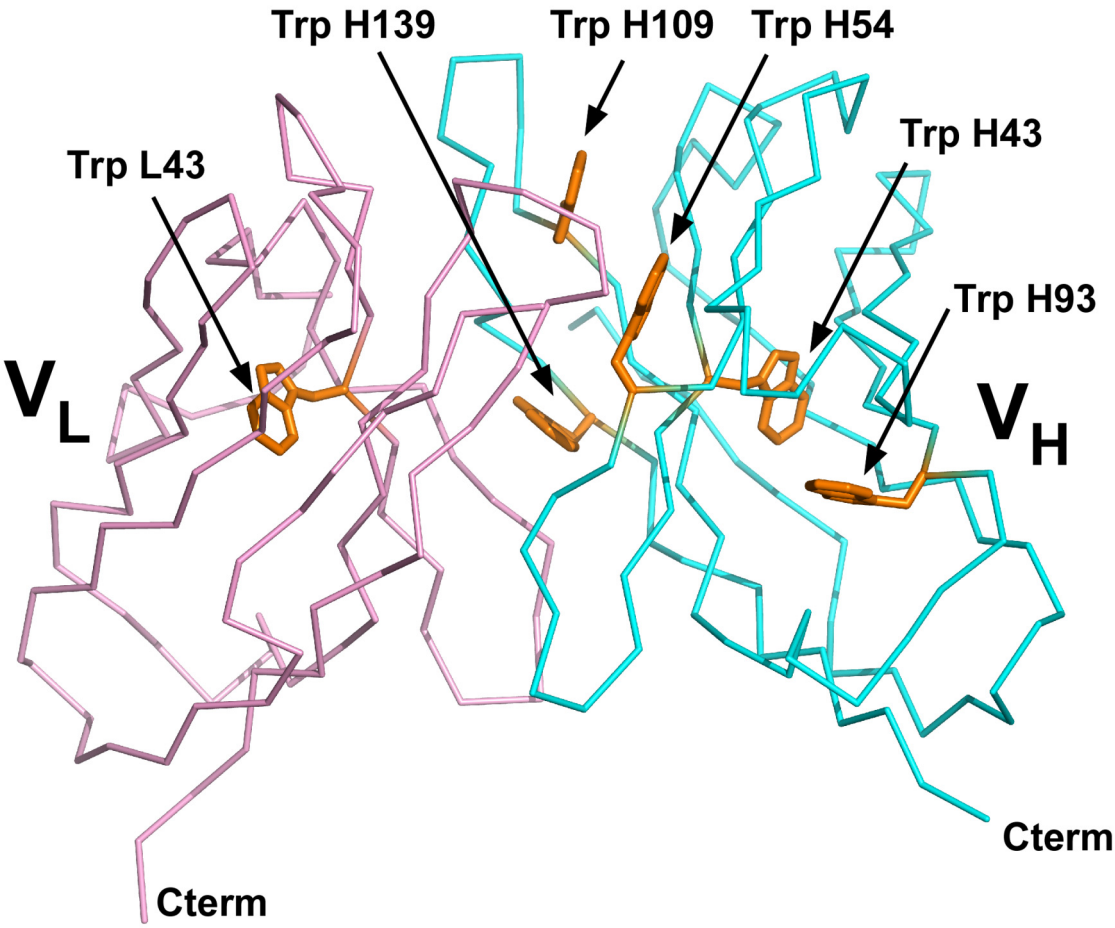

Figure S1: Positions of tryptophan residues in the scFv fragment: Constructs huV$_\kappa$3-huV$_H$3, huV$_\kappa$3-huV$_H$3•MocB and huV$_\kappa$3-huV$_H$3•1 contain 5 Trp residues: Trp L43 is fully quenched in the native state, the same is probably true for Trp H43. Three Trp residues are mostly buried in the interface between V$_L$ and V$_H$: Trp H54 (conserved), Trp H109 (CDR-H3) and Trp H139 (conserved). They become solvent exposed when either domain unfolds. Construct huV$_\kappa$3-huV$_H$3•5 contains a sixth Trp, H93, which is fully buried in the V$_H$ core.

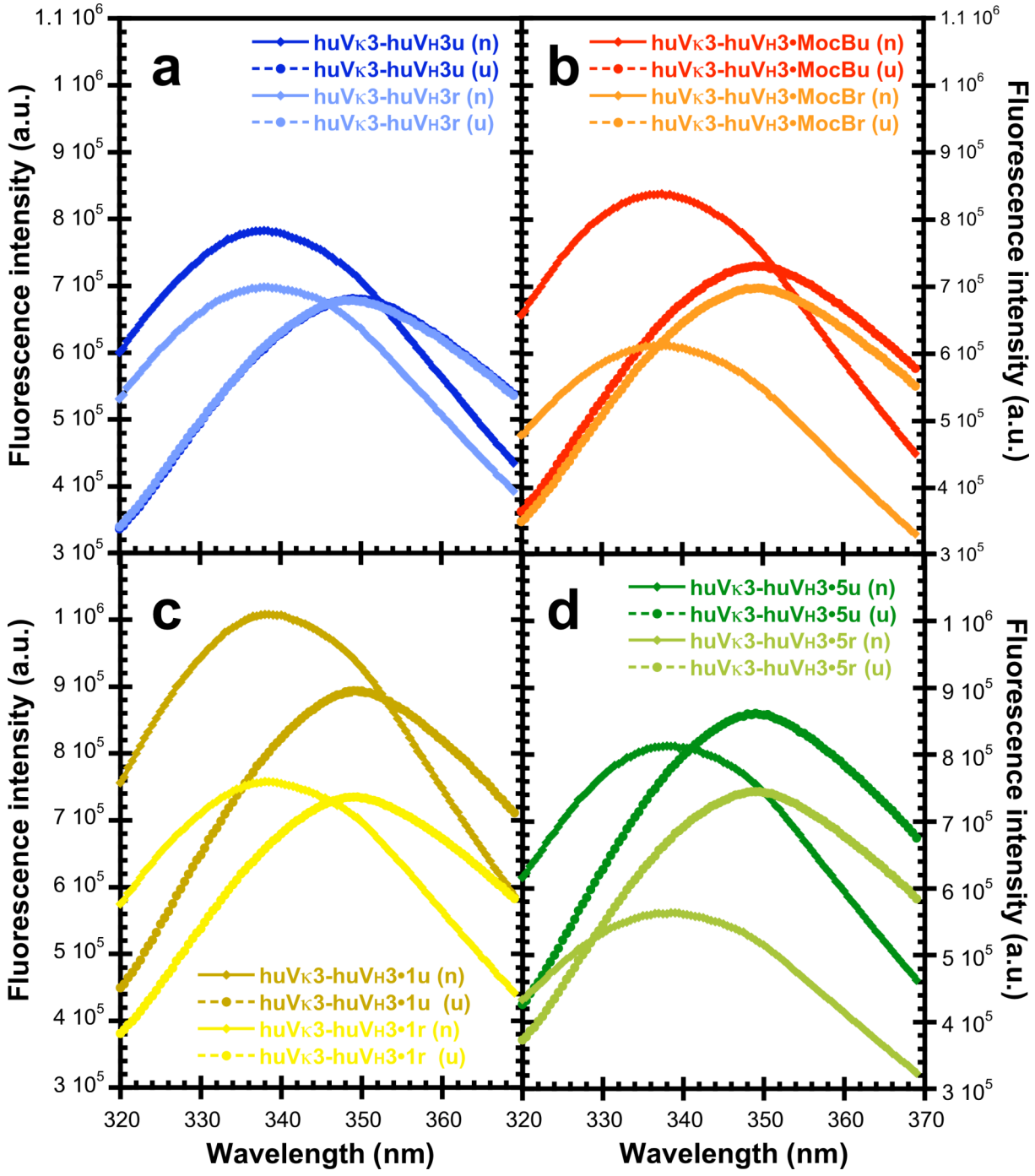

Figure S2: Fluorescence spectra of the scFv fragments huV$_\kappa$3-huV$_H$3 **(a)**, huV$_\kappa$3-huV$_H$3•MocB **(b)** and huV$_\kappa$3-huV$_H$3•1 **(c)** and huV$_\kappa$3-huV$_H$3•5 **(d)** at low (0 - 0.2 M GdmCl (n)) and high (4.9-5.1 M GdmCl, (u)) denaturant concentration. Comparison of the corresponding spectra taken from the unfolding curve (e.g. huVκ3-huV$_H$3u) and from the refolding curve (e.g. huVκ3-huV$_H$3r) demonstrate the variations of the fluorescence intensities, but the reproducibility and reversibility of λ_{max} (cf. the normalized spectra in Figure S3)

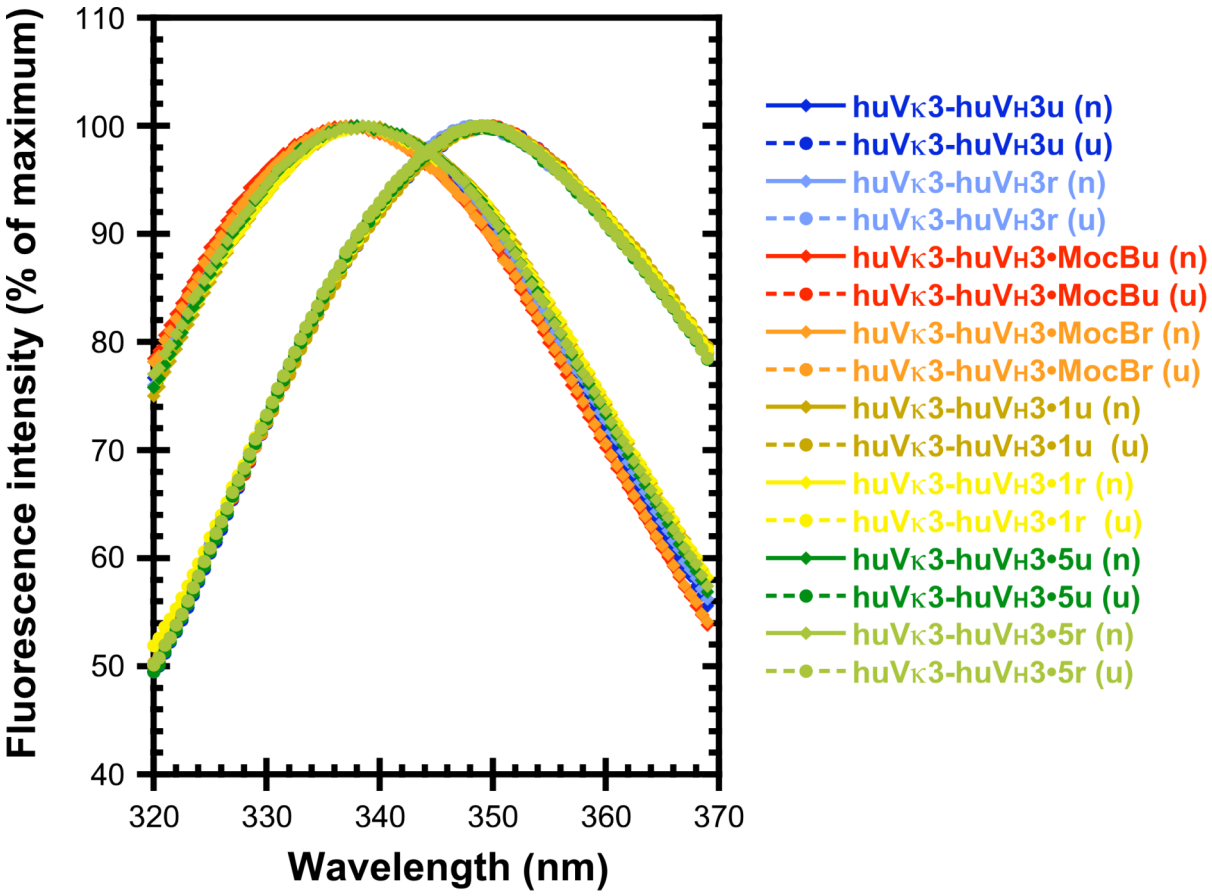

Figure S3: Normalized fluorescence spectra. The spectra shown in Figure S2 were normalized at the maximal fluorescence intensity to show that the shape and wavelength of the fluorescence maxima of the unfolded spectra is the same for all constructs, while the wavelength of the fluorescence maxima of the native spectra differ slightly for the different constructs.

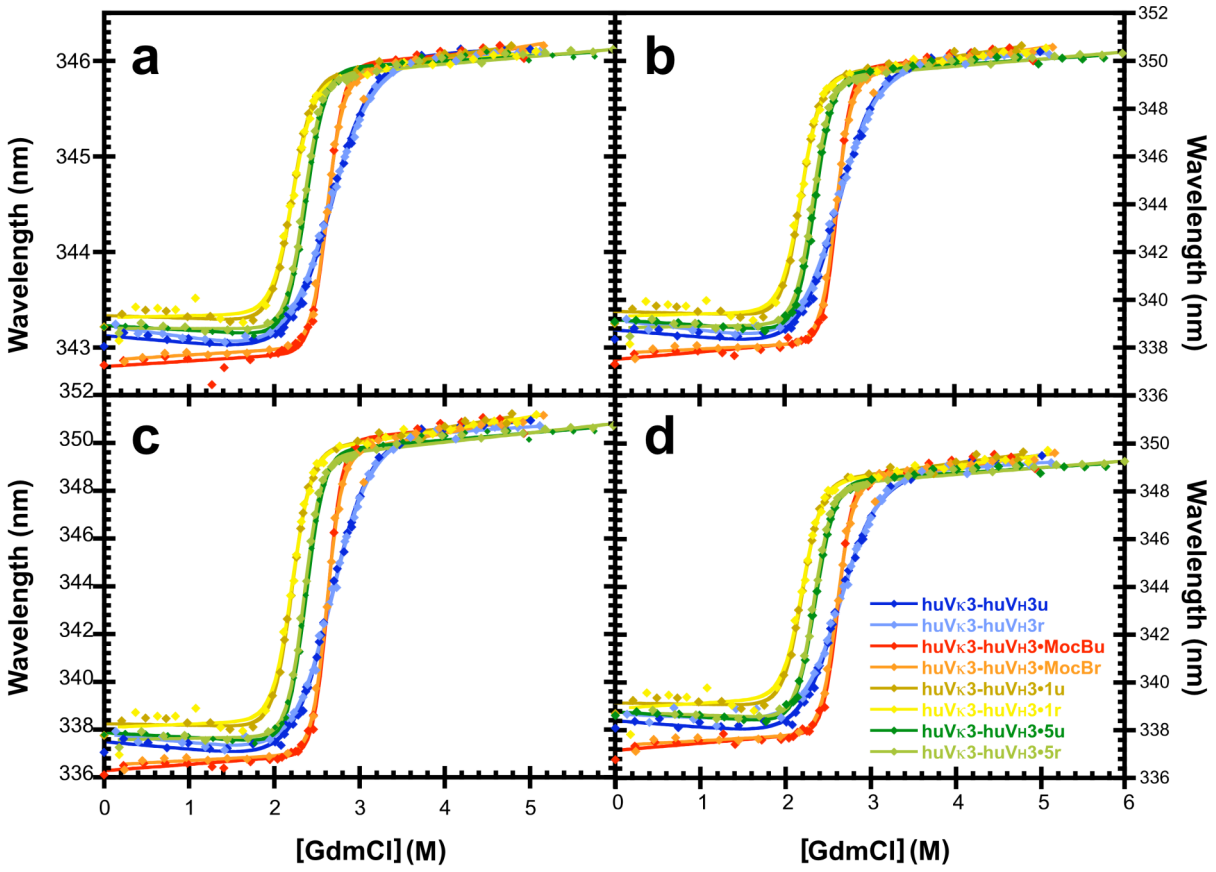

Figure S4: Equilibrium unfolding curves. For each of the four scFv in the study, both the equilibrium unfolding curves (u) and the equilibrium refolding curves (r) starting from material equilibrated for 24 h in 6 M GdmCl were determined. The spectral shifts upon denaturation were determined by different methods and fitted according to eq. 1 (main text, Materials and Methods) (Creighton, 1997). The parameters derived from this fit are listed in Table ST1

(a) Center of spectral mass (csm) plotted against the denaturant concentration. The csm over the interval from 320 to 370 nm is determined as the sum of each fluorescence intensity at a given wavelength multiplied by this wavelength, divided by the sum of the fluorescence intensities over this interval. The csm makes no assumptions concerning the shape of the fluorescence spectrum.

(b) Wavelength of the emission maximum determined by fitting a Gaussian curve to the fluorescence peak over the interval from 320 to 370 nm. This is a deliberately poor choice, as we usually use a narrower interval to more precisely fit the peak maximum, but it still leads to very similar curves.

(c) Wavelength of the emission maximum determined by fitting a Taylor series to the third order term (Monsellier and Bedouelle, 2005)

(d) Wavelength of the emission maximum determined by fitting a Taylor series to the fourth order term (Monsellier and Bedouelle, 2005)

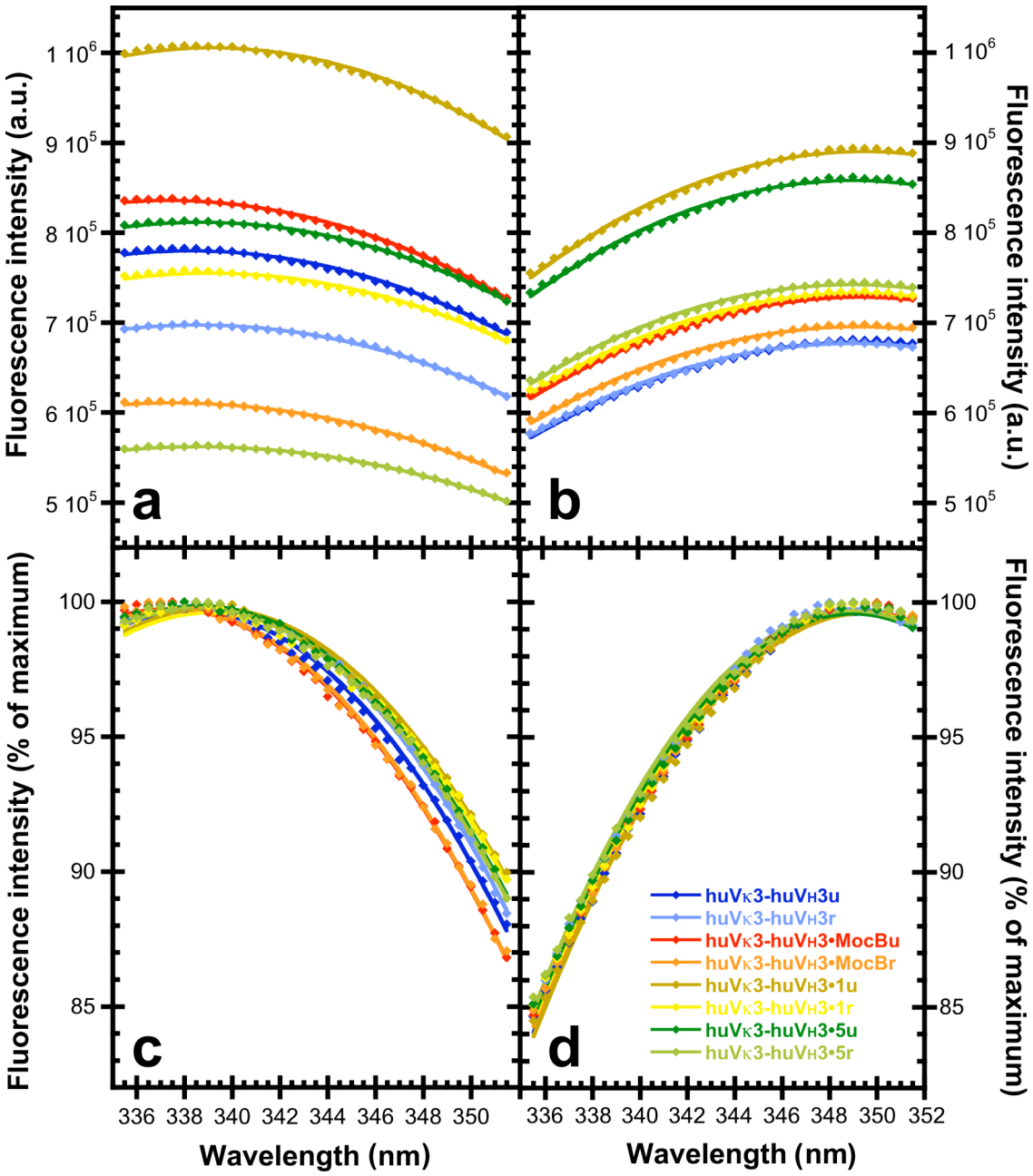

Figure S5: Curvature of the spectra shown in Figures S2 and S3. λ_{max}(n) and λ_{max}(u) of each construct were determined by fitting a Taylor series to the fourth order term to the spectra in the wavelength interval from 320 to 370 nm. The curvature was then determined by fitting the spectra with a parabola, centered on λ_{max}(n) or λ_{max}(u), respectively, in the wavelength interval from λ_{max}(n) – 2 nm to λ_{max}(u) + 2 nm according to Monsellier and Bedouelle (2005). **(a)** Spectra of native scFv, **(b)** spectra of denatured scFv **(c)** spectra of native scFv normalized to 100% intensity at λ_{max}, **(d)** spectra of denatured scFv normalized to 100% intensity at λ_{max}. The parameters derived from (a) and (b) are listed in Table ST3, together with the $\Delta G_{(H2O)}$-correction derived from this fit according to Monsellier and Bedouelle (2005). The values derived from (c) and (d) are given in Table ST3 for illustration only.

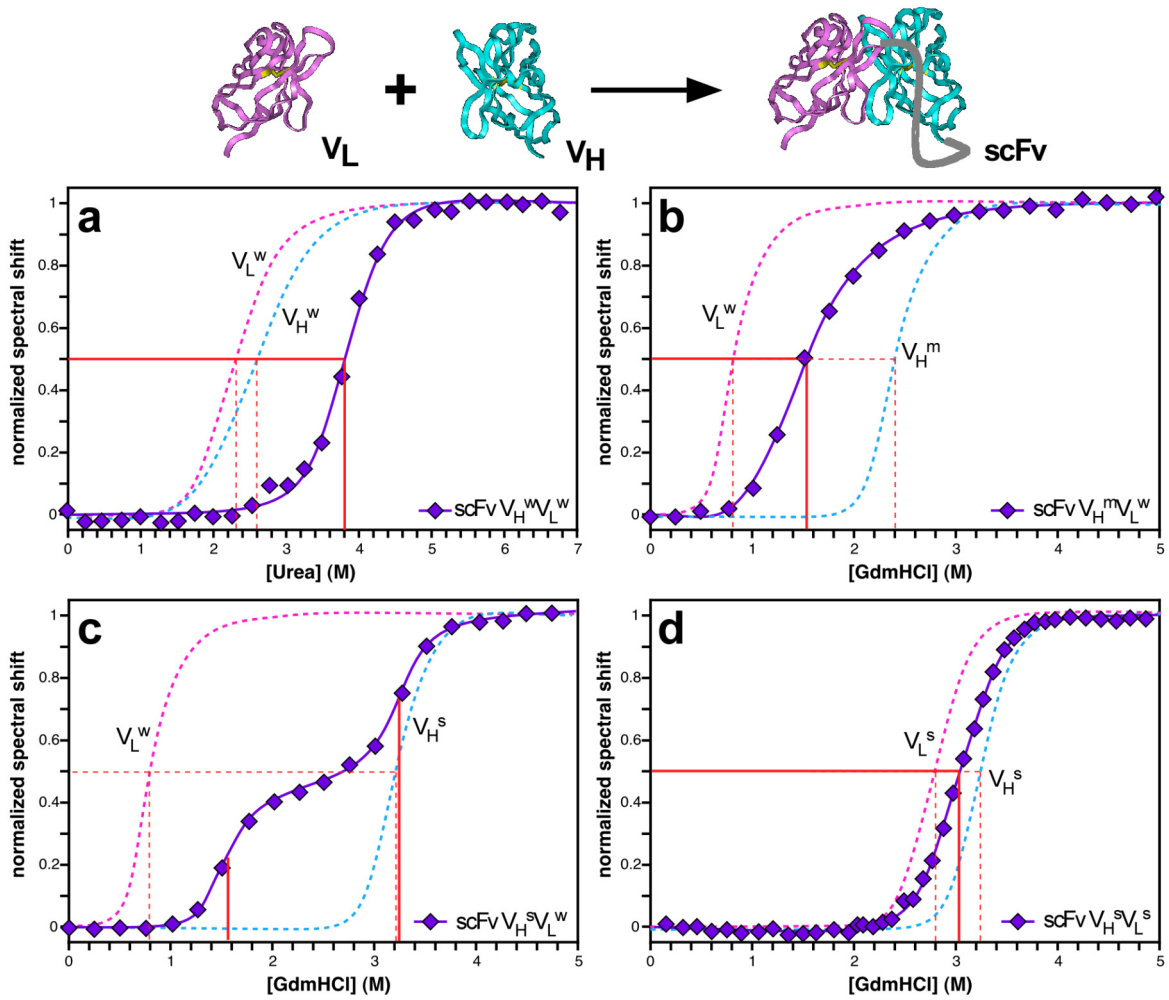

Figure S6: Two-state and non two-state systems. Cooperativity of scFv unfolding curves as a function of the intrinsic stabilities of the constituent domains (redrawn from the data of Wörn and Plückthun (1999); Röthlisberger *et al.*, (2005)).

(a) Unfolding of a weak V_L domain (*w.t.* AB48) is coupled to a weak V_H domain (disulfide-free AB48 Cys H23 Ala) in V_H-linker-V_L orientation. The resulting scFv shows a cooperative equilibrium unfolding curve with a midpoint at significantly higher denaturant concentration than the midpoints of either of the two constituent domains (indicated by dashed lines).

(b) A weak V_L domain (*w.t.* AB48) is coupled to a V_H domain of intermediate stability (disulfide-free AB48 Lys H77 Arg, Asn H59 Ser, Tyr H106 Val). The resulting scFv shows an equilibrium unfolding curve with apparent low cooperativity (broad transition) and a midpoint denaturant concentration intermediate between those of the two constituent domains.

(c) A weak V_L domain is coupled to a very strong V_H domain (disulfide-restored AB48 Lys H77 Arg, Asn H59 Ser). The unfolding curve of the scFv shows a clear equilibrium unfolding intermediate; although the unfolding curve of the V_L domain is shifted to higher denaturant concentrations than that of the free V_L domain, the V_L in the scFv fully unfolds at denaturant

concentrations at which V_H has not even started to unfold. The unfolding curve of the V_H domain within the scFv is not affected by the presence of the V_L domain.
(d) A very strong V_L domain (4D5) is coupled to a very strong V_H domain (disulfide-restored AB48 Lys H77 Arg, Asn H59 Ser). The resulting scFv shows an equilibrium unfolding curve with apparent low cooperativity and a midpoint denaturant concentration intermediate between those of the two constituent domains

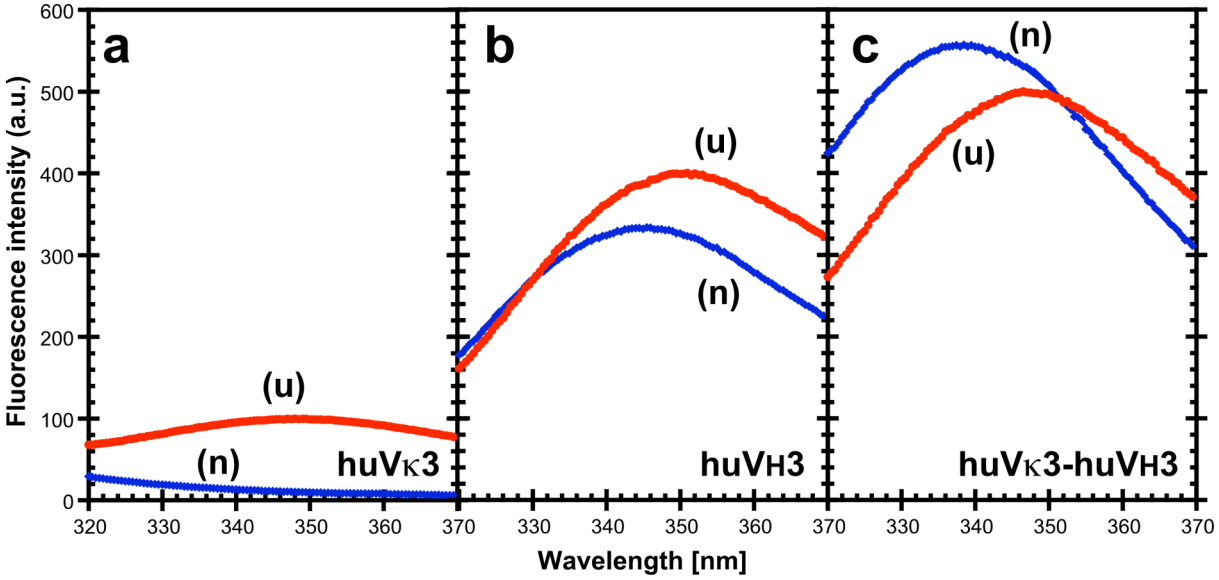

Figure S7: Fluorescence emission spectra of the isolated domains huVκ3 and huV$_H$3 in native and denatured form, compared to the scFv huVκ3-huV$_H$3. The scales of the three panels have been adjusted to make the peak intensity of the fully denatured proteins (red curves, (u)), proportional to the number of tryptophan residues in each construct (since those spectra are essentially dominated by exposed Trp). The spectra of the native proteins (blue curves, (n)) are properly scaled in relation to their denatured counterparts, as experimentally determined. **(a)** The V_L domain contains a single Trp (L43) that is fully quenched in the native state. **(b)** The fluorescence spectrum of the native V_H domain (4 Trp) is dominated by the three Trp that in the scFv are buried in the V_L/V_H interface. In the isolated domain, these Trp are partially solvent-exposed. The core Trp H43 presumably is quenched to a similar extent as the core Trp of the V_L domain. **(c)** The intensity of the fluorescence emission of the native scFv is significantly higher than the sum of the emissions of the isolated domains. Since the three interface Trp are mostly buried in the scFv, the wavelength of the emission maximum of the native scFv is shifted to lower wavelengths compared to the isolated V_H domain. Upon unfolding of the scFv fragment, two effects come into play: first, the core Trp residues of V_L and V_H become unquenched, resulting in an increased fluorescence of the isolated domains. Second, fluorescence quantum yield of the interface Trp residues decreases, when this interface is destroyed. Both effects somewhat compensate each other, such that the overall quantum yield at the respective maxima of the native and unfolded scFv fragment is not very different (blue and red curves in (c)). See Figure S1 for the location of the Trp residues in the scFv structure. Fitted λmax and curvatures are listed in Table ST4. The Figure was produced using raw data from Ewert *et al.* (2003).

Table ST1: Fit of a two-state model of the unfolding transition to the data depicted in Figure S4, using different fitting approaches

		λ max(n) nm	slope(n) nm*L/mol	λ max(u) nm	slope (u) nm*L/mol	ΔG(H2O) J/mol	m J*L/mol^2	R
a	huVκ3-huVH3u	**343.1** ± 0.03	**-0.078** ± 0.029	**345.9** ± 0.17	**0.053** ± 0.039	**27610** ± 1139	**10394** ± 430	0.9993
	huVκ3-huVH3r	**343.2** ± 0.03	**-0.127** ± 0.026	**345.9** ± 0.12	**0.038** ± 0.026	**25597** ± 820	**9688** ± 309	0.9996
	huVκ3-huVH3•MocBu	**342.8** ± 0.04	**0.058** ± 0.028	**345.7** ± 0.17	**0.083** ± 0.043	**67230** ± 6181	**25608** ± 2368	0.9989
	huVκ3-huVH3•MocBr	**342.9** ± 0.05	**0.055** ± 0.036	**345.4** ± 0.10	**0.147** ± 0.025	**69012** ± 5019	**26384** ± 1898	0.9990
	huVκ3-huVH3•1u	**343.3** ± 0.03	**-0.029** ± 0.027	**345.5** ± 0.07	**0.130** ± 0.019	**45284** ± 1998	**20528** ± 901	0.9995
	huVκ3-huVH3•1r	**343.3** ± 0.06	**0.020** ± 0.063	**345.5** ± 0.14	**0.113** ± 0.034	**44677** ± 4952	**20214** ± 2212	0.9976
	huVκ3-huVH3•5u	**343.2** ± 0.03	**-0.050** ± 0.023	**345.8** ± 0.05	**0.052** ± 0.012	**51072** ± 2034	**21556** ± 850	0.9995
	huVκ3-huVH3•5r	**343.2** ± 0.04	**-0.004** ± 0.030	**345.7** ± 0.04	**0.078** ± 0.010	**54612** ± 2604	**23254** ± 1097	0.9993
b	huVκ3-huVH3u	**338.7** ± 0.13	**-0.301** ± 0.123	**348.6** ± 0.68	**0.370** ± 0.159	**29328** ± 1376	**11203** ± 527	0.9991
	huVκ3-huVH3r	**339.2** ± 0.13	**-0.430** ± 0.125	**348.9** ± 0.51	**0.289** ± 0.118	**27758** ± 1159	**10627** ± 440	0.9993
	huVκ3-huVH3•MocBu	**337.5** ± 0.12	**0.314** ± 0.073	**348.7** ± 0.45	**0.369** ± 0.113	**79782** ± 5718	**30447** ± 2185	0.9994
	huVκ3-huVH3•MocBr	**337.8** ± 0.15	**0.182** ± 0.112	**347.9** ± 0.30	**0.533** ± 0.077	**70040** ± 4038	**26903** ± 1536	0.9994
	huVκ3-huVH3•1u	**339.5** ± 0.11	**-0.093** ± 0.113	**348.1** ± 0.30	**0.525** ± 0.078	**48651** ± 2437	**22191** ± 1107	0.9994
	huVκ3-huVH3•1r	**339.3** ± 0.28	**0.102** ± 0.272	**348.3** ± 0.56	**0.436** ± 0.142	**45981** ± 5648	**20965** ± 2537	0.9972
	huVκ3-huVH3•5u	**339.2** ± 0.10	**-0.225** ± 0.088	**349.0** ± 0.19	**0.223** ± 0.045	**53020** ± 2123	**22510** ± 892	0.9995
	huVκ3-huVH3•5r	**338.8** ± 0.12	**0.064** ± 0.106	**348.6** ± 0.15	**0.301** ± 0.034	**55022** ± 2438	**23587** ± 1033	0.9994
c	huVκ3-huVH3u	**337.5** ± 0.14	**-0.317** ± 0.128	**349.0** ± 0.76	**0.399** ± 0.177	**29282** ± 1287	**11016** ± 486	0.9992
	huVκ3-huVH3r	**337.8** ± 0.16	**-0.351** ± 0.139	**349.6** ± 0.65	**0.221** ± 0.149	**28695** ± 1236	**10742** ± 461	0.9993
	huVκ3-huVH3•MocBu	**336.3** ± 0.13	**0.266** ± 0.080	**349.0** ± 0.50	**0.389** ± 0.123	**77096** ± 5218	**29323** ± 1986	0.9995
	huVκ3-huVH3•MocBr	**336.5** ± 0.24	**0.192** ± 0.177	**347.7** ± 0.48	**0.670** ± 0.123	**72313** ± 6046	**27641** ± 2288	0.9987
	huVκ3-huVH3•1u	**338.3** ± 0.13	**-0.067** ± 0.124	**348.3** ± 0.34	**0.590** ± 0.088	**49417** ± 2353	**22404** ± 1062	0.9994
	huVκ3-huVH3•1r	**338.1** ± 0.29	**0.148** ± 0.275	**348.4** ± 0.58	**0.537** ± 0.148	**47654** ± 5206	**21600** ± 2331	0.9978
	huVκ3-huVH3•5u	**337.9** ± 0.12	**-0.196** ± 0.099	**348.9** ± 0.23	**0.296** ± 0.053	**54483** ± 2272	**22996** ± 951	0.9995
	huVκ3-huVH3•5r	**337.6** ± 0.13	**0.067** ± 0.111	**348.5** ± 0.15	**0.389** ± 0.036	**58312** ± 2390	**24818** ± 1007	0.9995
d	huVκ3-huVH3u	**338.4** ± 0.13	**-0.267** ± 0.118	**347.1** ± 0.65	**0.493** ± 0.152	**29041** ± 1427	**11127** ± 549	0.9990
	huVκ3-huVH3r	**338.7** ± 0.15	**-0.155** ± 0.139	**348.0** ± 0.61	**0.232** ± 0.140	**28832** ± 1556	**10895** ± 585	0.9989
	huVκ3-huVH3•MocBu	**337.2** ± 0.13	**0.301** ± 0.084	**347.6** ± 0.52	**0.379** ± 0.130	**75301** ± 6173	**28779** ± 2369	0.9992
	huVκ3-huVH3•MocBr	**337.4** ± 0.18	**0.203** ± 0.133	**347.0** ± 0.35	**0.492** ± 0.091	**68696** ± 4876	**26417** ± 1857	0.9990
	huVκ3-huVH3•1u	**339.2** ± 0.12	**-0.056** ± 0.120	**347.3** ± 0.32	**0.468** ± 0.083	**47623** ± 2676	**21729** ± 1216	0.9992
	huVκ3-huVH3•1r	**338.9** ± 0.28	**0.220** ± 0.268	**347.4** ± 0.55	**0.425** ± 0.140	**46599** ± 6188	**21242** ± 2780	0.9969
	huVκ3-huVH3•5u	**338.8** ± 0.09	**-0.214** ± 0.078	**347.9** ± 0.17	**0.223** ± 0.039	**50386** ± 1838	**21490** ± 775	0.9996
	huVκ3-huVH3•5r	**338.8** ± 0.13	**-0.123** ± 0.104	**347.6** ± 0.12	**0.286** ± 0.027	**54184** ± 2036	**23243** ± 861	0.9996

*u = unfolding
*r = refolding from 6M GdmCl

The columns give the fitted parameters form a two-state interpretation of the data for the pre-transition baseline (intercept λ_{max}(n) and slope(n)), for the post-transition baseline (intercept λ_{max}(u) and slope(u)), the apparent free energy of unfolding $\Delta G_{(H2O)}$ extrapolated to zero denaturant and the apparent m-value (slope of extrapolation). Eq. 1 was used (in the main text), using the change of the relevant fluorescence wavelength as a function of denaturant. The letters (a, b, c, d) indicate which wavelength was used:

(a) Center of spectral mass of the fluorescence spectrum from 320 nm - 370 nm as a function of denaturant concentration

(b) Wavelength of the fluorescence maximum determined by a Gaussian fit of the fluorescence spectrum from 320 nm - 370 nm as a function of denaturant concentration

(c) Wavelength of the fluorescence maximum determined from a fit of the fluorescence spectrum from 320 nm - 370 nm by a Taylor expansion to the 3rd power term as a function of denaturant concentration

(d) Wavelength of the fluorescence maximum determined from a fit of the fluorescence spectrum from 320 nm - 370 nm by a Taylor expansion to the 4th power term as a function of denaturant concentration.

Table ST2: Comparison of the apparent $\Delta G_{(H2O)}$, m-values and $[GdmCl]_{50}$ derived from the fits shown in Figure S4 and Table ST1

		a	b	c	d
ΔG(H2O) kcal/mol	huVκ3-huVH3u	**6.6** ± 0.27	**7.0** ± 0.33	**7.0** ± 0.31	**6.9** ± 0.34
	huVκ3-huVH3r	**6.1** ± 0.20	**6.6** ± 0.28	**6.9** ± 0.30	**6.9** ± 0.37
	huVκ3-huVH3•MocBu	**16.1** ± 1.48	**19.1** ± 1.37	**18.4** ± 1.25	**18.0** ± 1.47
	huVκ3-huVH3•MocBr	**16.5** ± 1.20	**16.7** ± 0.96	**17.3** ± 1.44	**16.4** ± 1.16
	huVκ3-huVH3•1u	**10.8** ± 0.48	**11.6** ± 0.58	**11.8** ± 0.56	**11.4** ± 0.64
	huVκ3-huVH3•1r	**10.7** ± 1.18	**11.0** ± 1.35	**11.4** ± 1.24	**11.1** ± 1.48
	huVκ3-huVH3•5u	**12.2** ± 0.49	**12.7** ± 0.51	**13.0** ± 0.54	**12.0** ± 0.44
	huVκ3-huVH3•5r	**13.0** ± 0.62	**13.1** ± 0.58	**13.9** ± 0.57	**12.9** ± 0.49
m kcal*L/mol^2	huVκ3-huVH3u	**2.5** ± 0.10	**2.7** ± 0.13	**2.6** ± 0.12	**2.7** ± 0.13
	huVκ3-huVH3r	**2.3** ± 0.07	**2.5** ± 0.11	**2.6** ± 0.11	**2.6** ± 0.14
	huVκ3-huVH3•MocBu	**6.1** ± 0.57	**7.3** ± 0.52	**7.0** ± 0.47	**6.9** ± 0.57
	huVκ3-huVH3•MocBr	**6.3** ± 0.45	**6.4** ± 0.37	**6.6** ± 0.55	**6.3** ± 0.44
	huVκ3-huVH3•1u	**4.9** ± 0.22	**5.3** ± 0.26	**5.4** ± 0.25	**5.2** ± 0.29
	huVκ3-huVH3•1r	**4.8** ± 0.53	**5.0** ± 0.61	**5.2** ± 0.56	**5.1** ± 0.66
	huVκ3-huVH3•5u	**5.1** ± 0.20	**5.4** ± 0.21	**5.5** ± 0.23	**5.1** ± 0.19
	huVκ3-huVH3•5r	**5.6** ± 0.26	**5.6** ± 0.25	**5.9** ± 0.24	**5.6** ± 0.21
[D]50 mol/L	huVκ3-huVH3u	**2.7** ± 0.17	**2.6** ± 0.20	**2.7** ± 0.19	**2.6** ± 0.21
	huVκ3-huVH3r	**2.6** ± 0.12	**2.6** ± 0.17	**2.7** ± 0.18	**2.6** ± 0.23
	huVκ3-huVH3•MocBu	**2.6** ± 0.91	**2.6** ± 0.84	**2.6** ± 0.77	**2.6** ± 0.91
	huVκ3-huVH3•MocBr	**2.6** ± 0.75	**2.6** ± 0.60	**2.6** ± 0.90	**2.6** ± 0.72
	huVκ3-huVH3•1u	**2.2** ± 0.26	**2.2** ± 0.32	**2.2** ± 0.31	**2.2** ± 0.35
	huVκ3-huVH3•1r	**2.2** ± 0.65	**2.2** ± 0.74	**2.2** ± 0.69	**2.2** ± 0.81
	huVκ3-huVH3•5u	**2.4** ± 0.28	**2.4** ± 0.29	**2.4** ± 0.32	**2.3** ± 0.25
	huVκ3-huVH3•5r	**2.3** ± 0.36	**2.3** ± 0.34	**2.3** ± 0.33	**2.3** ± 0.28

*u = unfolding
*r = refolding from 6M GdmCl

The letters a, b, c and d indicate the method used to fit the spectra, as described in the legends to Figure S4 and Table ST1

Table ST3: Corrections to $\Delta G_{(H2O)}$ -values derived from the spectral shift for the different curvatures of the spectra of the native and the denatured scFv according to Monsellier and Bedouelle (2005).

Curvatures derived from raw spectra

	λmax (n)	λmax (u)	b(n)	b(u)	b(n)/b(u)	RT*ln(b(n)/(bu)) J/mol	kcal/mol
huVκ3-huVH3u	338.3	349.3	-1059	-1109	0.955	**-113**	**-0.03**
huVκ3-huVH3r	338.6	349.0	-949	-1118	0.849	**-400**	**-0.10**
huVκ3-huVH3•MocBu	337.3	349.3	-1085	-1174	0.924	**-192**	**-0.05**
huVκ3-huVH3•MocBr	337.5	349.2	-814	-1138	0.715	**-816**	**-0.19**
huVκ3-huVH3•1u	339.2	349.5	-1328	-1434	0.926	**-188**	**-0.04**
huVκ3-huVH3•1r	339.1	349.2	-979	-1183	0.827	**-462**	**-0.11**
huVκ3-huVH3•5u	338.7	349.0	-1061	-1412	0.751	**-697**	**-0.17**
huVκ3-huVH3•5r	338.6	348.9	-728	-1219	0.597	**-1258**	**-0.30**

Curvatures derived from normalized spectra (for illustration only)

	λmax (n)	λmax (u)	b(n)	b(u)	b(n)/b(u)	RT*ln(bn/bu) J/mol	kcal/mol
huVκ3-huVH3u	338.3	349.3	-0.135	-0.163	0.831	**-450**	**-0.11**
huVκ3-huVH3r	338.6	349.0	-0.136	-0.165	0.825	**-469**	**-0.11**
huVκ3-huVH3•MocBu	337.3	349.3	-0.130	-0.161	0.806	**-526**	**-0.13**
huVκ3-huVH3•MocBr	337.3	349.2	-0.133	-0.163	0.815	**-498**	**-0.12**
huVκ3-huVH3•1u	337.5	349.5	-0.132	-0.160	0.821	**-480**	**-0.11**
huVκ3-huVH3•1r	339.1	349.2	-0.129	-0.161	0.802	**-537**	**-0.13**
huVκ3-huVH3•5u	338.7	349.0	-0.130	-0.164	0.796	**-555**	**-0.13**
huVκ3-huVH3•5r	338.6	348.9	-0.129	-0.164	0.789	**-578**	**-0.14**

*u =unfolding
*r = refolding from 6M GdmCl

The terms b(n) and b(u) are defined in Monsellier and Bedouelle (2005). Curves derived from normalized spectra are only shown to demonstrate that the variability in the curvature-derived ΔG correction terms is entirely due to the large error in the fluorescence intensities and not due to changes in the shape of the spectrum.

Table ST4: Emission maxima of the native and the unfolded state and curvatures for the native and denatured isolated V_L and V_H domain shown in Figure S7 compared to the scFv.

	λmax(n)	λmax(u)	b(n)	b(u)	b(n)/b(u)
huVk3	**n.d.**	**348.3**	n.d.	-0.121	**n.d.**
huVH3	**345.1**	**350.4**	-0.585	-0.667	**0.877**
huVk3-huVH3	**338.5**	**347.2**	-0.747	-0.814	**0.918**

Since the core Trp is fully quenched in the native state of huVκ3 (see Figure S7), λmax (n), b(n) and b(n)/b(u) could not be determined (nd). Therefore, the spectral shift cannot be used to evaluate the stability of the isolated V_L domain. However, isolated V_L domains are much less prone to aggregation than V_H domains, permitting the use of fluorescence intensity to monitor unfolding. Since the interface Trp are solvent exposed in the isolated V_H domain, the spectral shift upon unfolding is much smaller than for the scFv.